International Journal of Multiphase Flow 114 (2019) 19–27

Contents lists available at ScienceDirect

International Journal of Multiphase Flow

journal homepage: www.elsevier.com/locate/ijmulflow

Pore-scale modelling of gravity-driven drainage in disordered porous media

Guanzhe Cui[a], Mingchao Liu[a,b], Weijing Dai[a], Yixiang Gan[a,*]

[a] School of Civil Engineering, The University of Sydney, NSW 2006, Australia
[b] Department of Engineering Mechanics, CNMM & AML, Tsinghua University, Beijing 100084, China

ARTICLE INFO

Article history:
Received 7 June 2018
Revised 7 January 2019
Accepted 9 February 2019
Available online 10 February 2019

Keywords:
Multiphase flow
Disordered porous media
Gravity-driven drainage
Bond number
Wettability

ABSTRACT

Multiphase flow through a porous medium involves complex interactions between capillarity, wettability and gravity during drainage process. In contrast to these factors, the effect of pore distribution on liquid retention is less understood. In particular, the quantitative correlation between the fluid displacement and the level of disorder has not yet been established. In this work, we employ direct numerical simulation by solving the Navier–Stokes equations and using volume of fluid method to track the liquid–liquid interface during drainage in disordered porous media. The disorder of pore configuration is characterized by an modified index to capture small microstructural perturbation, which is pivotal for fluid displacement in porous media. Then, we focus on the residual volume and morphological characteristics of saturated zones after drainage and investigate the effect of disorder under different wettability (i.e., the contact angle) and gravity (characterized by a modified Bond number) conditions. Pore-scale simulations reveal that the highly-disordered porous medium is favourable to improve liquid retention and provide various morphologies of entrapped saturated zones. Furthermore, the disorder index has a negative correlation to the characteristic curve index (n) in van Genuchten equation, controlling the shape of the retention characteristic curves. It is expected that the findings will benefit to a broad range of industrial applications involving drainage processes in porous media, e.g., drying, carbon sequestration, and underground water remediation.

1. Introduction

Drainage in porous media, a typical multiphase flow problem, plays a significant role in many environmental applications and industrial processes, including carbon capture and storage (CCS), oil and gas extraction, geological hazards, pharmaceutics, and food processes (Parker et al., 1987; Olivella et al., 1994; Bandara et al., 2011; Colombo and Fairweather, 2015; Zhao et al., 2016; Rabbani et al., 2017). As a wetting phase (e.g., liquid) is withdrawn and replaced by another non-wetting phase (e.g., gas), the flow phenomena and the distribution of the entrapped saturated zone are dominated by complex interactions among different constituents, including gas, liquid and solid, and attracting interests from different research areas related to unsaturated soil mechanics, groundwater remediation, and physics of porous media (Méheust et al., 2002; Islam et al., 2014; Ghanbarian et al., 2015).

The multiphase interactions combining several factors (including intrinsic topological features, gravity, capillary, and wettability) determine macroscopic drainage properties, such as the residual saturation of wetting phase and the temporal/spatial distributions of saturated zones (Yang et al., 1988; Herring et al., 2016; Li et al., 2018). The majority of previous experiments and numerical models of drainage and injection are focusing on the macroscopic parameters, e.g., porosity, permeability, system size and aspect ratio (Succi et al., 1989; Toussaint et al., 2005; Babadagli et al., 2015; Moura et al., 2015; Rognmo et al., 2017; March et al., 2018), in which the spatial configuration, pore connectivity and their influences on liquid retention are ignored (Prat, 1995; Lin et al., 2018; Yekta et al., 2018). However, for most natural and synthetic porous media, disordered microstructures are dominance (Anguy et al., 2001; Woo et al., 2004). These disorder features not only affect the mechanical properties of porous media (Laubie et al., 2017a, 2017b), but also hinder the fundamental understanding of drainage processes (Holtzman, 2016; Fantinel et al., 2017). Further studies are required to evaluate the degree of microstructural disorder and bridge the microscopic structure information to macroscopic effective properties of porous media.

Displacement efficiency of two-phase flow in disordered porous media is important in many applications

* Corresponding author.
E-mail address: yixiang.gan@sydney.edu.au (Y. Gan).

https://doi.org/10.1016/j.ijmultiphaseflow.2019.02.001
0301-9322/

(Dias and Payatakes, 1986). It has been found that the efficiency of immiscible fluids is influenced by the microstructure in those media (Zhao et al., 2016; Hu et al., 2018). For example, low disorder of porous geometry is found to be advantageous for fluid displacement in partially saturated porous media; on the other hand, in terms of liquid mixing and reaction, highly-disordered porous materials is desirable (Holtzman, 2016). These applications indicate that the disordered microstructure and its effects on liquid-liquid displacement need to be quantitatively assessed. However, the quantitative and systematic studies about the effect of disordered microstructure on the multiphase flow problems, particularly on liquid retention during drainage processes, remain relatively scarce.

In the past few years, increasing attention has been focused on the effect of disordered geometry on immiscible two-phase flow (Ferrari et al., 2015; Holtzman, 2016; Rabbani et al., 2017). The ordered and disordered porous media have clear differences in the behaviours and mechanisms of multiphase fluid displacement processes (Pak et al., 2015). With an increase of the disorder degree, the displacement stability is weakened, which results in a lower degree of saturation than that in relatively more homogeneous pore network (Liu et al., 2015). Ferrari et al. (2015) studied numerically the effect of different disordered microstructure controlled by a standard deviation of solid phase size on the unstable invasion structure in Hele–Shaw cells consisting of a large number of cylindrical obstacles. The quantitative assessment on the impact on the disorder of pore distribution keeps relatively unexplored.

In this paper, we employ the direct numerical simulation (DNS) by using the volume of fluid (VOF) method based on Eulerian algorithms to capture the detailed flow dynamics within the porous media, which describes the distribution of two phases as a fluid function with different properties. Then, quasi-two-dimensional (2D) simulations of gravity-driven drainage are performed on a broad range of scenarios and the temporal and spatial information of saturated clusters is exacted and analysed. Our objectives are twofold: firstly, we investigate the reliability of an introduced disorder index to characterize a quantitative relation between the degree of microstructural disorder and retention characteristics; secondly, we demonstrate the effect of gravitational force and wettability on drainage consequence under different disorder degree conditions.

2. Numerical modelling

In this section, we introduce the numerical framework for generating and characterizing the disordered porous media, via an improved disorder index using Voronoi tessellations of the pore space, and modelling the gravity-driven drainage processes by employing VOF method in *OpenFOAM (Greenshields, 2015)*.

2.1. Disorder index, I_v

To quantitatively investigate the influence of the degree of microstructural disorder in porous media on the drainage process, we explore a meaningful measure of the disorder of the pore space, as well as generating samples with the controlled disorder quantity. Here a model 2D porous medium containing mono-sized circular discs is focused, seen in Fig. 1(a). Random samples can be achieved by deviating the discs from the original regular arrangement, e.g., a hexagonal or square lattice. The porous medium is in form of N disk-shaped solid phases of radius R that is embedded in a rectangular plate of size $L_x \times L_y$ with the periodic boundary condition along the x-axis. The centers of discs are moved with a random vector $\overrightarrow{R_m}$ ($|\overrightarrow{R_m}| \leq \delta$, where δ is the maximum step for random moves). The disordered porous media contain only non-overlapping discs at a constant global porosity, ϕ, are constructed and the corresponding degree of disorder can be controlled by varying δ. The movement method of discs allows a larger range of configuration from the completely ordered system, $\delta = 0$, to highly-disordered systems by applying the moving steps iteratively. It should be noted that, as a first-order approximation of disordered porous medium, this 2D idealised system can reflect essential features of the disordered microstructure to facilitate more comprehensive investigations of the effects of the degree of disorder on drainage processes in the actual porous media, which may consist of other heterogeneous features, such as non-uniform pore shapes and interconnecting solid phase.

Since the porosity ϕ as a global parameter is determined by the number and size of discs in the domain, the next high-order parameter is a measurement of the fluctuations of local porosity ϕ_i, e.g., $I_d = [< \phi_i^2 > - \phi^2]^{1/2}$ as the index of disorder proposed by Laubie et al. (2017a). Note that the average operator $\langle \cdot \rangle$ is volumetric average. The local porosity ϕ_i is evaluated at every point i in a square background mesh of the domain with a mesh size of $l = (\pi R^2/\phi)^{1/2}$. However, in this paper, we observed that this original definition ignores the small microstructural perturbation which is pivotal for pore fluid flow (discussed later). Thus we propose here a modified index based on Voronoi tessellations of the pore space as the primitive volume, instead of the regular background square mesh, as shown in Fig. 1(b). The local porosity ϕ_i can be calculated in a tessellated volume cantered on in the ith pore. The modified disorder parameter ("disorder index"), I_v, takes the same format of the original definition, but uses the set $\{\phi_i\}$ based on Voronoi tessellations as

$$I_v = \left[< \phi_i^2 > - < \phi_i >^2 \right]^{1/2}. \quad (1)$$

Note here ϕ is replaced with the volume average sample porosity, $\langle \phi_i \rangle$. The parameter I_v can change from zero, an ordered geometry, to an approximate maximum value of 0.06 for a highly disordered porous structure. It is worth noting that here the maximum

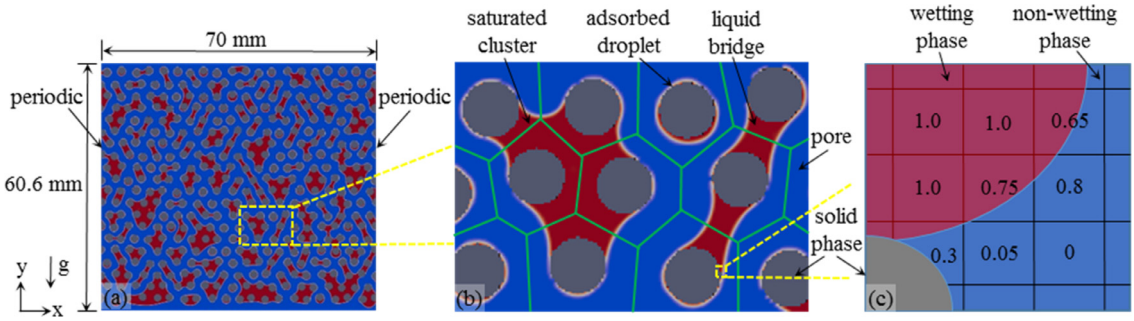

Fig. 1. Schematic diagrams of (a) a typical computational domain used for the drainage process containing solid (grey), liquid (red) and gas (blue) phases, (b) Voronoi tessellations on the pore space and three characteristic liquid zones (saturated cluster, adsorbed droplet and liquid bridge), (c) VOF method with the volume fraction of wetting liquid inside each square grid. (For interpretation of the references to colour in this figure legend, the reader is referred to the web version of this article.).

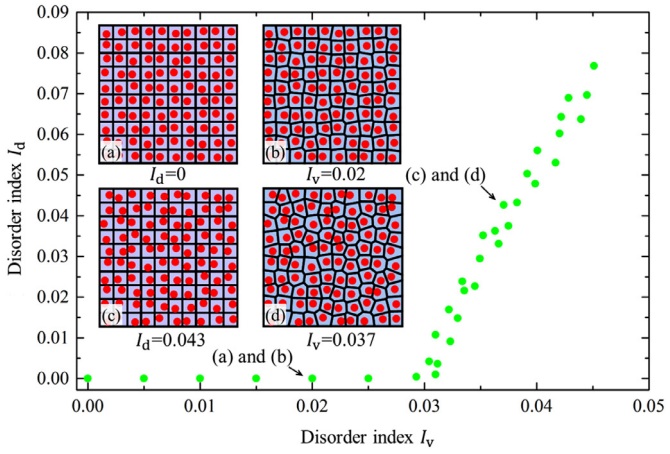

Fig. 2. The comparison between disordered indices I_d (original definition) and I_v (modified index). Inserts (a)–(d) indicate the different background meshes used for calculating the local porosity: (a) $I_d = 0$ and (b) $I_v = 0.02$, (c) $I_d = 0.043$ and (d) $I_v = 0.037$, where (a and b) and (c and d) are two cases with identical pore structure.

value is only related to the specific method adopted for generating the disordered structure, i.e., moving the disc centres with a random vector and limiting the vector to remove the possible overlaps of discs. A larger value of I_v can be achieved by adopting another generating method for the disordered geometry.

Fig. 2 shows the comparison between two disorder indices, I_d and I_v. When the ordered primitive structure is slightly disturbed, e.g., $\delta \leq l/2 - R$, $I_d = 0$, while I_v varies from 0 to 0.03. The reason is that, when the circular discs only randomly move within the square meshes, the local porosity ϕ_i equals to mean global porosity ϕ, as shown in Fig. 2(a)–(d) of the two identical microstructures. This indicates that I_d cannot be used to characterize the small variation in a unit cell (as mentioned as "Randomness Case I" in Laubie et al. (2017b)); on the contrary, the modified definition using Voronoi tessellation is sensitive to such small disturbances. However, this limited movement has a quite significant impact on the drainage processes, which will be demonstrated later in Section 3. Moreover, the resulting ranges of I_d and I_v also differ from $I_d \in [0, 0.1]$ and $I_v \in [0, 0.06]$, respectively. As a result, for investigating the pore-scale multiphase flow in this paper, we employed the I_v based on Voronoi tessellations to evaluate the degree of microstructural disorder in porous media.

2.2. Volume of fluid

In traditional computational fluid dynamics, during the procedure of solving the Navier–Stokes equations, it is extremely difficult and computationally expensive to solve moving interfacial boundary condition problems (Horgue et al., 2013). However, the VOF method employs treatments of two immiscible, isothermal, and incompressible liquid phases as a single-fluid phase with different properties including density and viscosity. It utilizes an additional interfacial force replacing the jump condition at the liquid–liquid interface (Owkes and Desjardins, 2014). In VOF method, the process of drainage in porous media can be described as a wetting phase ("defending fluid") replaced by a non-wetting phase ("invading fluid") (Ferrari and Lunati 2013).

The spatial distribution of two immiscible fluid phases is described as the phase indicator for fluids, shown in Fig. 1(c), as

$$\alpha = \begin{cases} 0 & \text{in the non} - \text{wetting (nw) fluid,} \\ 1 & \text{in the wetting (w) fluid.} \end{cases} \tag{2}$$

According to the dynamic law of fluid phase, the immiscible fluids can be expressed by the conversation of mass and momentum as a set of Navier–Stokes equations:

$$\nabla \cdot \boldsymbol{u} = \boldsymbol{0}, \tag{3}$$

$$\frac{\partial \rho \boldsymbol{u}}{\partial t} + \nabla \cdot (\rho \boldsymbol{u}\boldsymbol{u}) = -\nabla p + \nabla \cdot (2\mu \boldsymbol{E}) + \boldsymbol{f}_s, \tag{4}$$

where $\boldsymbol{u}$ is the fluid velocity, p is the pressure, $\boldsymbol{E} = \frac{1}{2}(\nabla u + \nabla u^T)$ is the strain rate tensor, ρ and μ are the density and viscosity considering multiple fluid phases, respectively, as:

$$\rho(\boldsymbol{x}) = \alpha\rho_w + (1-\alpha)\rho_{nw}, \tag{5}$$

$$\mu(\boldsymbol{x}) = \alpha\mu_w + (1-\alpha)\mu_{nw}, \tag{6}$$

In Eq. (4), the last term represents the effect of Laplace pressure at the interface and is defined as:

$$\boldsymbol{f}_s = 2\gamma k \boldsymbol{n} \delta_T, \tag{7}$$

where γ is the interfacial tension between the two fluids, δ_T is a unit function that is 0 in the whole domain except at the interface, $\boldsymbol{n}$ is the normal to the interface, and k is the mean curvature at the interface:

$$k = \frac{1}{2}\nabla \cdot \boldsymbol{n} = \frac{1}{2}\nabla \cdot \left(\frac{\nabla \alpha}{\| \nabla \alpha \|} \right), \tag{8}$$

In this work, the no-slip condition is adopted, i.e., the vectorial component of velocity is zero on the solid boundary. To reproduce the wetting behaviour at the triple line region, the boundary condition in VOF equals to Young's law as defined as (Ferrari and Lunati, 2013):

$$\boldsymbol{n}|_{\delta_r} = \boldsymbol{t_s}\sin\theta + \boldsymbol{n_s}\cos\theta, \tag{9}$$

where $\boldsymbol{n}$ is the normal to two fluids interface at the solid surface (δ_r), $\boldsymbol{t_s}$ is the unit tangent toward the wetting phase, $\boldsymbol{n_s}$ is the unit normal pointing into the solid, and θ is the contact angle. When the above equations are used to compute the whole-domain velocity field and describe the evolution of the fluid-fluid displacement, the advection equation should be included as

$$\frac{\partial \alpha}{\partial t} + \nabla \cdot (\alpha \boldsymbol{u}) + \nabla \cdot (\boldsymbol{u}_r \alpha(1-\alpha)) = 0, \tag{10}$$

where $\boldsymbol{u}_r$ ($\boldsymbol{u}_r = \boldsymbol{u}_1 - \boldsymbol{u}_2$) is the relative velocity between the two fluids. Since *OpenFOAM* use the surface compression method to implement the VOF method, the second term on the left hand side is an artificial compression term applied to prevent the numerical diffusion which smears the sharp interface (Boyce et al., 2016).

2.3. Simulation setup and materials parameters

The numerical simulations are implemented in an open-source CFD platform, *OpenFOAM*, with a multiphase flow solver *interFoam*. This solver employs Finite Volume (FV) schemes for the discretization of partial differential equations to calculate multiple immiscible fluids phases. Inside the pore space, the classical Navier–Stokes equations are solved by VOF method tracking the temporal and spatial evolution of fluid–fluid interface. A mesh generator, *snappyHexMesh*, is used to automatically generate complex meshes of hexahedral and split-hexahedral cells from triangulated surface geometry in the domain. In order to construct a quasi-2D model, the out-of-plane thickness of the sample is particularly set to be much smaller than the in-plane edges in x and y axis. The initial background hexagonal mesh is iteratively refined to better reproduce the cylindrical surface with the meshes.

To investigate the morphological characteristics of entrapped wetting fluid, including adsorbed liquid, liquid bridge and saturated cluster, as shown in Fig. 1(b), we simulated drainage under atmospheric condition in a rectangular domain (Fig. 1(a)) with

Table 1
Geometrical parameters of the quasi-two-dimensional porous media and properties of two immiscible fluids used in numerical simulations.

Property	Value
Radius of discs, R (mm)	1
Contact angle, θ (°)	0°∼150°
Kinematic viscosity of wetting phase (m^2/s)	5.93×10^{-7}
Kinematic viscosity ratio, μ_w/μ_{nw} (-)	0.38
Density of wetting phase, ρ_w (kg/m^3)	997
Density of non-wetting phase, ρ_n (kg/m^3)	11.69
Density difference, $\Delta\rho$ (kg/m^3)	985.31
Void ratio, e (-)	2.65
Gravity acceleration, g (m/s^2)	9.81
Surface tension, γ (N/m)	0.064

Table 2
A sensitivity study on the domain size based on the same discretization $2R/\Delta = (27)$.

	Small	Medium	Large
Dimensions (mm^2)	35×52.32	70×96.13	140×193.25
Number of discs (-)	100	400	1600
Number of meshes (-)	825,547	2975,769	11,990,042
Porosity (-)	0.704	0.705	0.704
Degree of residual saturation	17.73%	16.90%	14.94%

Table 3
A sensitivity study on discretization based on the medium-sized domain.

	Discretisation, $2R/\Delta$			
	16	27	32	41
Number of meshes (-)	1080,298	2.975,769	5268,631	6662,617
Porosity (-)	0.704	0.705	0.705	0.708
Degree of residual saturation	15.86%	16.90%	17.11%	16.93%

inlet on top, outlet on bottom and periodic boundary condition in the horizontal direction. The geometrical parameters of computational models are shown in Table 1. The dynamics of fluid-fluid displacement, morphology and distribution of wetted zone during gravity-driven drainage depend on the properties of wetting and non-wetting phases including density, viscosity and surface tension, shown in Table 1. These values are selected based on the parameters of water and air under 25 °C and 1 MPa ambient pressure, which take into account the underground environment adopted in previous studies (Ferrari and Lunati, 2013).

Before the detailed simulation of drainage processes, we have performed convergence analysis on the mesh discretization and domain size to identify the cost-efficient mesh density and representative model size. A compromise between the level of discretization and size of computational domains has to be found. To this end, we tested several cases including three computational domains and four levels of discretization, defined by the ratio of disc diameter to typical mesh cell size (i.e., $2R/\Delta$ = 16, 27, 32, 41). The benchmark is defined in terms of the residual saturation at the end of gravitational drainage process, and all cases are conducted under the same porosity and pore structure, with $\theta = 30°$ and Bond number of 0.36. Based on these results (shown in Tables 2 and 3), we decided to select the case with medium domain size of 70×96.13 mm^2 with 400 solid discs and discretisation of$2R/\Delta = (27)$ (meshes), which ensures that differences with the results obtained with the finest mesh discretization and largest domain size are within 3%.

2.4. A modified bond number

During the gravity-driven drainage process, the interplay between the gravity and capillary forces has a significant effect on the fluid displacement behaviours. In order to quantify the relative magnitude of these two forces, a dimensionless parameter, i.e., the Bond number, is introduced in the previous work (Méheust et al., 2002; Moebius and Or, 2014) as

$$B_o = \frac{\Delta\rho g a^2}{\gamma}, \tag{11}$$

where a is the characteristic length, $\Delta\rho$ the density difference between wetting and non-wetting phases and g the gravity acceleration. The characteristic length is usually defined as the throat size (Blunt and Scher, 1995) or the radius of pore (Birovljev et al., 1991; Løvoll et al., 2005). However, because the disorder degree introduces non-uniform solid disc separations, the throat size is not easy to quantify. Here we adopt the uniform radius of solid discs as the characteristic length. In order to consider the variation due to the void ratio, we introduce the volumetric ratio between the pore and solid phase into the traditional form Eq. (12) and obtain the modified Bond number:

$$B_o' = \frac{\Delta\rho g R^2}{\gamma} \cdot e, \tag{12}$$

where R is the radius of the solid disc and $e = V_P/V_S$ is the void ratio, in which V_P and V_S are the total volume of pore and solid phase, respectively.

To demonstrate the validity of the modified Bond number, the parameters including the density difference, the gravity acceleration, the radius of solid disc, the void ratio are individually adjusted with the surface tension to keep the B_o' the same at 0.37. Fig. 3 demonstrates that the degree of saturation is similar when the B_o' is kept the same for given contact angle, across a range of wettability. The degree of saturation is a ratio of the residual volume of wetting phase to the void volume. Note that all the models are simulated under the same boundary conditions, as previously described in Section 2.3. In addition to the geometry (e = 2.65), the other two geometries (e = 1.50 and 1.63) are achieved by varying distances between discs and radius of discs (1 and 1.2 mm). In the Section 3.3, we will focus on the combined effects among the modified Bond number, disorder and wettability.

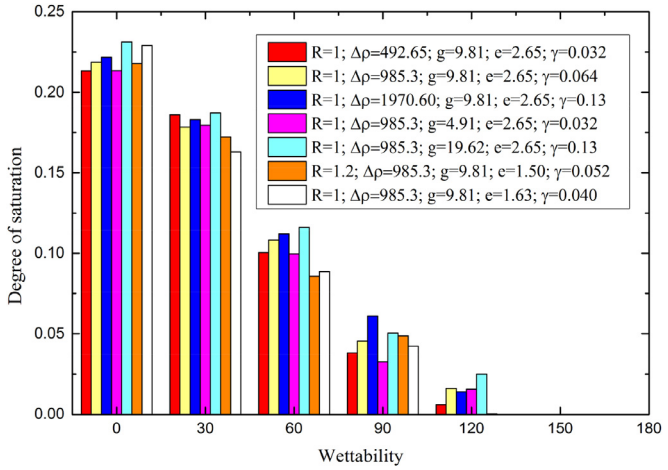

Fig. 3. Degree of residual saturation as a function of wettability (i.e., contact angle θ = 0, 30°, 60°, 90° and 120°) at $B_o' = 0.37$ with a different combination of density difference ($\Delta\rho$, kg/m^3), gravity acceleration (g, m/s^2), disc radius (R, mm), void ratio (e) and surface tension (γ, N/m).

3. Results analysis

By employing the proposed numerical model in the last section, we can investigate the gravity-driven drainage processes. More specifically, in this section, the effects of degree of disorder, gravity

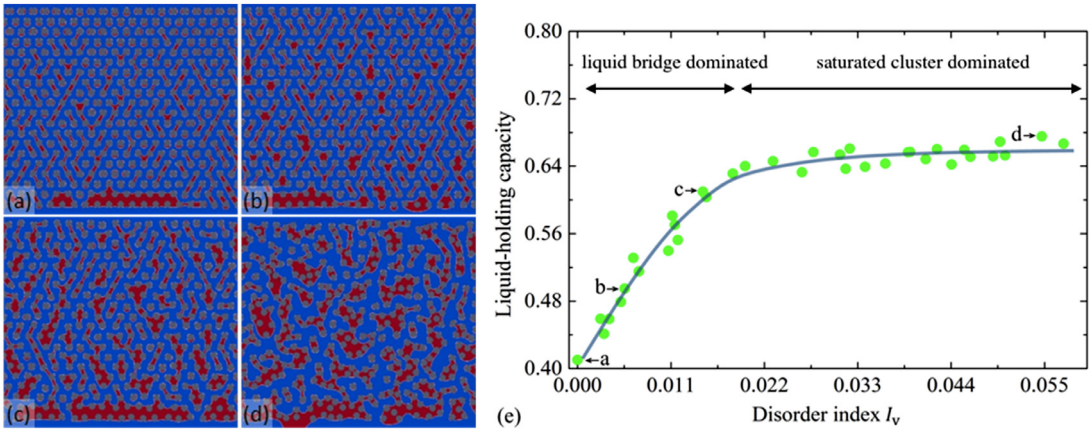

Fig. 4. Simulation results of four different samples at contact angle $\theta = 30°$ with increasing disorder index: (a) $I_v = 0$, (b) $I_v = 0.0056$, (c) $I_v = 0.015$ and (d) $I_v = 0.055$. (e) Liquid-holding capacity (the residual volume of wetting phase normalized by the solid volume as a function of disorder index I_v). The scale shows the range of liquid-holding capacity varying from 0.41 to 0.68.

and wettability on the residual volume and morphology distribution of wetting phase will be discussed.

3.1. Effects of disorder index, I_v

We first demonstrate the reliability of disorder index I_v by characterizing the effect of disorder degree of pore topology on the liquid-holding capacity, which is defined as the residual volume of wetting phase normalized by the solid volume. The liquid-holding capacity is more sensitive than degree of saturation to evaluate the effect of disordered degree on the average residual volume of circular discs. Note that, in order to exclude upper and lower boundary effects in the calculation, the volume of residual liquid within the top one row and bottom two rows of discs are removed during image processing. Fig. 4(a)–(d) show the spatial distributions of liquid zones (i.e., the entrapped saturated zones) in four samples with different pore topologies after drainage, which correspond to disorder index: $I_v = 0$ (ordered distribution), $I_v = 0.0056$, $I_v = 0.015$ and $I_v = 0.055$ (highly-disordered topology), respectively.

The morphological characteristics of entrapped saturated zones are significantly different in the four samples. Such variations in the morphology of the entrapped saturated zones at pore-scale will be analysed in detail in Section 3.2. In the macroscopic scale, the numerical results demonstrate that the degree of disorder has a monotonously increasing relationship with the volume of entrapped saturated zones, as shown in Fig. 4(e), in which the solid line is for a guiding purpose. It is interesting to note that the dependency of liquid-holding capacity drastically changes around $I_v \approx 0.02$, which represents a small perturbation or a relatively narrow pore size distribution. Below this degree of disorder, i.e., I_v varies in the range from 0 to 0.02, a more significant impact of I_v on the liquid-holding capacity than the rest range. Adsorbed droplets are rapidly connected into liquid bridges and even saturated clusters with the increasing degree of disorder within this range, which are more efficient to enhance the liquid-holding capacity than the other I_v range that mainly contains clusters. Note that I_d in the corresponding range keeps nearly zero when I_v vary from 0 to 0.02 (see Fig. 2), failing to capture this transition region.

When the degree of disorder is above the transition value (i.e., $I_v > 0.02$), the discs start to form clusters which coalesce the adjacent pores and result in a shift in the forms of liquid retention, i.e., a shift from liquid bridge dominated to saturated cluster dominated regime. In this range, the liquid-holding capacity tends to converge. Specifically, from Fig. 4e, an approximately saturated value 0.66 for liquid-holding capacity can be observed. The theoretical maximum for this liquid holding capacity represents the ratio between total pore and solid volumes, being 2.39 for the porosity of 0.705 used in this study. For a given drainage condition, e.g., at different Bond number, the variation is studied later in Section 3.3. These results indicate that the parameter I_v is effective to quantitatively evaluate the influence of the topological disorder on the liquid holding capacity. In addition, the increase of the disorder index is unfavourable for drainage efficiency in porous media.

3.2. Distribution of residual saturation cluster

In this section, the study aims to find a relationship between the disorder degree and the morphological characteristics of entrapped saturated zones after drainage. The spatial information of the saturated clusters is extracted by image processing. In statistics, the area of liquid bridges range from 0.8 mm^2 to 4 mm^2, and other zones of smaller or larger areas correspond to adsorbed droplets and saturated clusters, respectively, with typical examples shown in Fig. 1(b). In the post-processing, the extremely small liquid volume with a size smaller than one-tenth of a solid disc area (π mm^2) volume is neglected.

The probability density distribution of saturated zones volume after drainage processes are plotted in Fig. 5(a)–(d), corresponding to the pore topologies in Fig. 4(a)–(d) at contact angle 30°, respectively. The distributions of zone area using a uniform bin-width of 0.4 mm^2 are extracted from four samples with different disorder degree (i.e., $I_v = 0$, $I_v = 0.0056$, $I_v = 0.015$ and $I_v = 0.055$). Fig. 5(a) shows that, when the solid discs are assigned regularly ($I_v = 0$), the maximum probability of cluster area is possessed by the bin from 0.4 mm^2 to 0.8 mm^2, which is mostly consisted of the adsorbed droplets. In Fig. 5(b) and (c), the span of the size distribution of saturated zones becomes wider with increasing disorder of pore structure. Specifically, three kinds of wetting phase morphology (adsorbed droplet, liquid bridge and saturated cluster) simultaneously exist at the final drainage stages. When disorder index arrives the approximately maximum value (i.e., $I_v = 0.055$), the saturated zones in the highly-disordered porous media have the maximum cluster area reaching 40 mm^2 as well as the minimum number of adsorbed droplets and liquid bridges (see Fig. 5(d)). It should be noted that, in order to make the four sub-figures more visible and comparable, the maximum cluster area 40mm^2 is not displayed in Fig. 5(d) at the tail of the probability distribution. These results demonstrate that the increase of disorder contributes to the packaging of solid discs, which is advantageous for the merging of

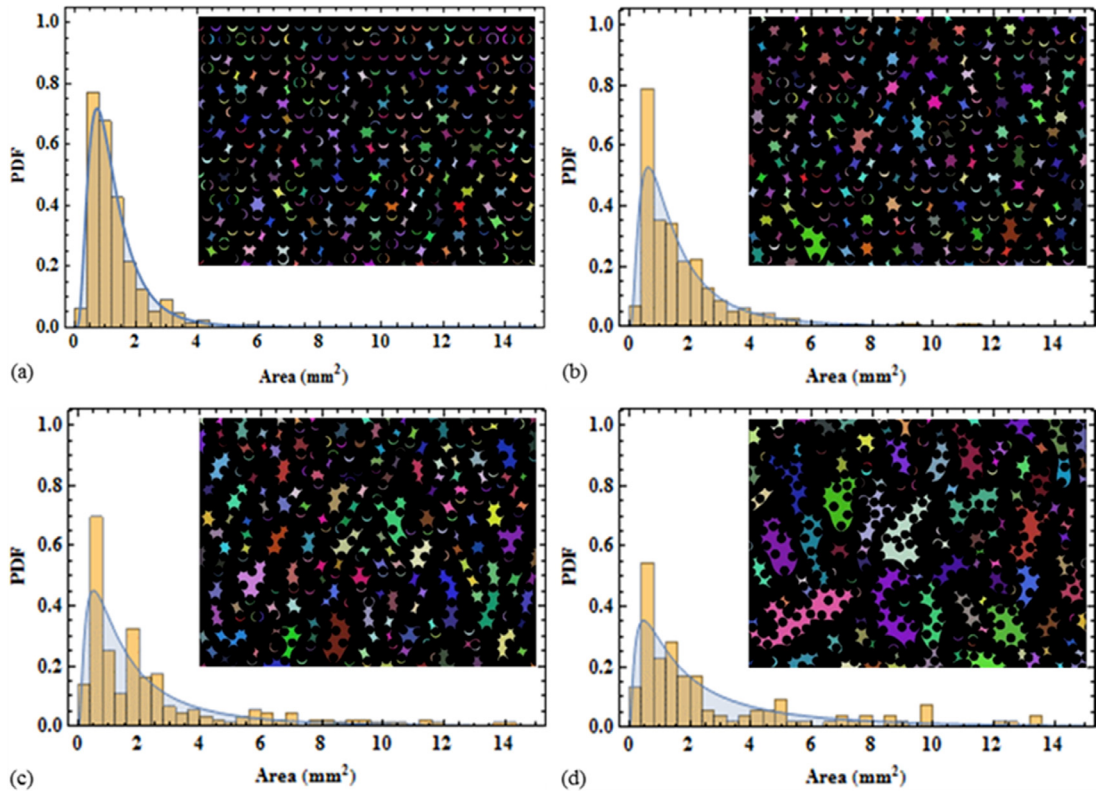

Fig. 5. Probability density function (PDF) and lognormal distribution of saturated zones area and maps of morphological characteristics with the four disorder parameters: (a) $I_v = 0$, $\mu = -0.061$, $\sigma = 0.59$; (b) $I_v = 0.0056$, $\mu = 0.24$, $\sigma = 0.85$; (c) $I_v = 0.015$, $\mu = 0.38$, $\sigma = 1.04$; (d) $I_v = 0.055$, $\mu = 0.66$, $\sigma = 1.20$. Note that the different colours in the inserted morphological character map represent the disconnected wetting phase zones.

adsorbed droplets into liquid bridges and further into residual saturated clusters.

Li et al. (2018) investigated cluster distribution during drainage experiments with 2D granular media and demonstrated that the dataset can be characterized by employing the lognormal distribution function, which has been employed in interpreting experimentally observed saturation clusters as

$$f(X|\mu,\sigma^2) = \frac{1}{\sqrt{(2\pi\sigma^2)X}}\exp\left[-\frac{(\ln X-\mu)^2}{2\sigma^2}\right]. \quad (13)$$

According to the maximum likelihood estimation method, two determinative parameters, i.e., the scale parameter (μ) and the shape parameter (σ), can be obtained by fitting the probability density distribution of liquid zone areas. It is clearly seen from Fig. 5(a) to (d) that the mean μ and variance σ have a positive relationship with the disorder index, indicating the increase of the mean and variation of residual liquid areas of high degree of disorder by enhancing the formation of saturated clusters. The reason is that a large I_v improves the solid phase packaging, individual liquid bridges and adsorbed droplets merging and eventually leading to the formation of large saturated zones in those dense regions. This further illustrates why the liquid-holding capacity is gradually enhanced with the increase of disorder degree and how the disorder of porous media statistically varies the total volume and morphological characteristics of residual wetting phase after the gravity-driven drainage process.

3.3. Liquid retention under varying bond number

To elucidate the combined effect of disorder degree and the modified Bond number, B_o', simulations are performed for the four disordered samples as shown in Fig. 4(a)–(d) with a broad range of B_o' from 0.011 to 7.70. The liquid-holding capacity of the disordered samples is plotted in Fig. 6 as a function of B_o'. The results demonstrate that, based on the influence of disorder, the drainage process can be divided into two categories, the capillary regime and adsorbed regime. The B_o' threshold separating these two categories is approximately 1.0, beyond which the gravitational force overtakes capillary force in drainage process, resulting in the disappearance of saturation clusters and capillary bridges.

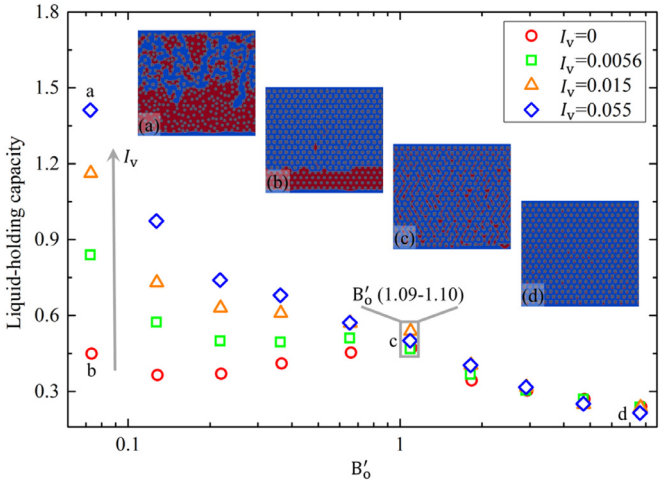

Fig. 6. Liquid-holding capacity as a function of Bond number with four different disorder indices and maps of wetted cluster distribution at contact angle $\theta = 30°$: (a) $I_v = 0.055$, $Bo' = 0.073$, (b) $I_v = 0$, $Bo' = 0.073$, (c) $I_v = 0$, $Bo' = 1.10$, (d) $I_v = 0.027$, $Bo' = 7.65$.

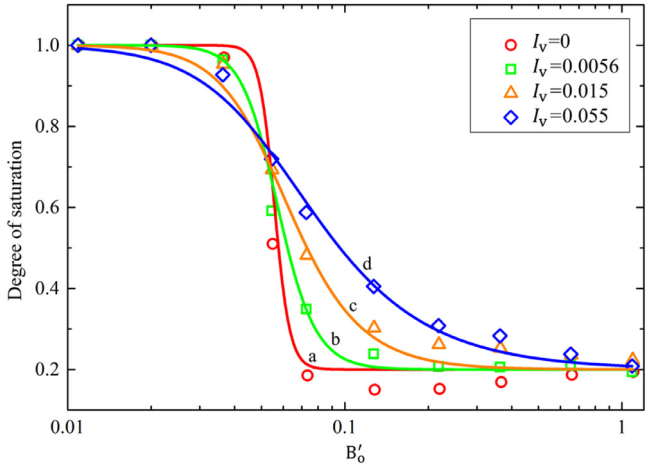

Fig. 7. Degree of residual saturation as a function Bond number fitted by van Genuchten equation (with $\alpha = 0.055$, $S_r^a = 0.20$): (a) $I_v = 0$, $n = 16.07$, (b) $I_v = 0.0056$, $n = 6.80$, (c) $I_v = 0.015$, $n = 3.75$, (d) $I_v = 0.055$, $n = 2.54$).

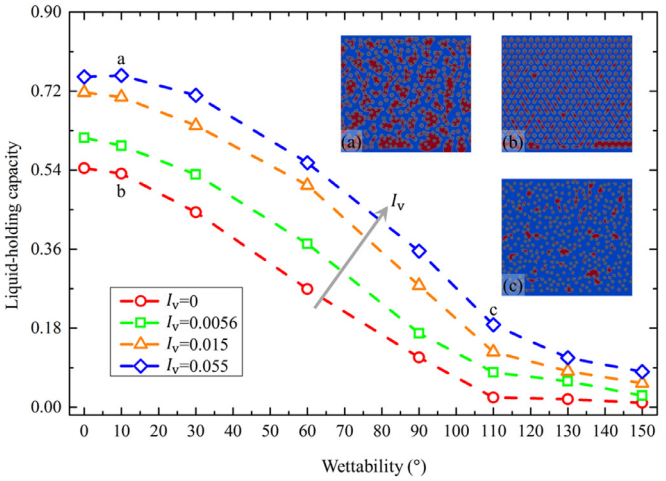

Fig. 8. Liquid-holding capacity as a function of wettability for the different disorder degree and morphological patterns of drainage results with different wettability conditions as inserts: (a) $I_v = 0.055$, $\theta = 10°$ (b) $I_v = 0$, $\theta = 10°$; and (c) $I_v = 0.055$, $\theta = 110°$.

When B_o' is less than the threshold, capillarity dominates the fluid-fluid displacement. Based on comparison between the ordered and the highly disordered medium (see Fig. 6(a) and (b)), higher disorder can dramatically improves the liquid-holding capacity of porous media with the same B_o'; in contrast to the only small adsorbed droplets in the ordered system, high disorder leads to large entrapped saturated zones, which demonstrates that disorder degree has a significant effect on the capillary interaction during drainage. In addition, it can be clearly seen that there is a morphological transformation from saturated zones (Fig. 6(a)) to liquid bridge (Fig. 6(c)) with the increasing gravitational force, which is consistent with the previous experimental results from Li et al. (2018).

In the second regime, i.e. $B_o' > 1.0$, the gravitational force has overcome the capillary counterpart. Fig. 6(d) indicates that only the adsorbed droplets exist on the surface of solid discs instead of the saturated patch and liquid bridges between discs in Fig 6(b) and (c), respectively. The adsorbed volume gradually declines with the increase of Bond number. Since the adsorbed liquid phase is only proportional to the total surface area (length in 2D) of the solid phase, there is no observed difference for ordered and disordered pore spaces, exhibiting similar relationship as shown in Fig. 6.

The van Genuchten equation originally describes the relationship between the degree of saturation and matric suction in the soil-water characteristics curves (SWCCs) (Zhou et al., 2016). As an analogue, here the residual volume is governed by the interaction between the capillary and gravitational forces (characterized by Bond number). Thus, we replaced the suction term in the original format with the Bond number:

$$S_r = \frac{1 - S_r^a}{\left[1 + \left(B_o'/\alpha\right)^n\right]^{1-1/n}} + S_r^a, \tag{14}$$

where S_r is the degree of saturation, S_r^a the adsorbed saturation, α the scaling parameter positively proportional to the potential value (here corresponding to B_o') of initial invasion of non-wetting phase, and n is the characteristic curve index controlling the slope of SWCC (Fredlund et al., 2012). Fig. 7 shows that the liquid retention curve can be quantitatively predicted by the van Genuchten equation (i.e., Eq. (15)). Furthermore, we conclude that with the same porosity and solid disc diameter, the increase of disorder index I_v decreases the curve index n. During the curve fitting process, we used $\alpha = 0.055$ and $S_r^a = 0.20$, since the former was found to be insensitive to I_v and latter can be measured at $B_o' = 1$. Thus, the potential relationship between the disorder of pore space and liquid characteristic curves can be evaluated quantitatively by the application of I_v under the framework of unsaturated soil mechanics.

3.4. Surface wettability

It is well known that the wettability of porous media can dramatically change the liquid-liquid displacement behaviour during both drainage and imbibition processes (Zhao et al., 2016), but whether the disorder alters such influence of wettability has not yet been explored. To this end, a series of simulations were performed on the disordered porous samples with the wettability of solid surface varying over a broad range from 0° to 150° at the same Bond number of 0.37. The results are plotted in Fig. 8. It is clearly seen that, with the increase of disorder index I_v, the volume of liquid retention is gradually elevated at the same wettabilities, which indicates the influence of the wettability on retention can be controlled by adjusting the disorder index (see Fig. 8(a) and (b)). Meanwhile, as for varying wettability, it is relatively more efficient to alter the residual volume when the disorder index is within $I_v \in (0–0.02)$, than the larger degree regime, $I_v \in (0.02–0.06)$. Due to the disorder-induced reinforcement of liquid-holding capacity, the maximum and minimum relative difference, compared to the ordered configuration at the same wettability, are 108% at the hydrophilic ($\theta = 60°$) and 716% at hydrophobic ($\theta = 150°$) samples, respectively.

In addition, when the surface wettability of porous media varies from hydrophilic to hydrophobic, wetting phase begins to flow out more and the liquid-holding capacity drastically decreases until approximately the inflection point (i.e., $\theta \sim 110°$). With the increase of hydrophobicity from 110° to 150°, such entrapment can be noticeably strengthened in high disorder samples and eventually keeps the residual volume of wetting phase non-zero. This entrapment phenomena can be explained after the pore invasion analysis by Cieplak and Robbins (1990) using the invasion pressure. The throat invasion pressure has a minimum pressure when the contact angle is larger than 90° and becomes significant around 110° During this transition, in terms of high disorder degree, the morphological characteristics of final drainage clearly transforms from a variety of liquid clusters to only entrapped droplets between the circular solid phase (see Fig. 8(c)). When the contact angle is within 0° to

110°, the effect of wettability on drainage efficiency is more obvious.

4. Disucussions

Our numerical results have shown that the modified disorder parameter I_v is reliable to quantitatively characterize the influence of disorder degree on liquid retention in porous media after the gravity-driven drainage process. The residual volume has a monotonously increasing relationship with the disorder index under the same porosity and radius of solid discs. It demonstrates that highly-disordered media is disadvantageous for drainage efficiency, however, the efficiency can be more sensitively controlled within the range of disorder index I_v (0–0.02) than the larger range (0.02–0.06).

For representing the morphological characteristics, we employed the lognormal function to fit the probability density distribution of saturated areas. The scale parameters μ and shape parameter σ are positively correlated with disorder index I_v, which indicates that enhancing disorder is advantageous for the formation of large fluid clusters. Due to the reinforcement of solid phase packaging, a large quantity of adsorbed droplets and liquid bridges can be gradually connected into liquid clusters. Moreover, for estimating the disorder influence on the resulting interfacial area after the drainage process, one can find that with the increase of disordered degree, the residual volume of wetting phase gradually rises up (as shown in the Fig. 4), which in principle enlarges the total interfacial area. Then, with the additional information regarding the cluster distribution (shown in Fig. 5), the actual interfacial area, although not quantitatively, can be estimated by the probability distribution of the saturated zones.

In addition, a modified Bond number, including the void ratio, is introduced. Based on the magnitude of gravitational and capillary forces, the drainage process is divided into two categories and the transition point of is approximately $B_o^{'} = 1.0$. When the gravitational force dominates the drainage process ($B_o^{'} > 1.0$), only adsorbed droplets exist on the solid surface without the presence of saturated clusters and liquid bridges, resulting in almost the same liquid-holding capacity for different disorder degree; on the other hand, when capillary force is larger than gravitational force ($B_o^{'} < 1.0$), the relationship between the degree of saturation and Bond number can be well represented by van Genuchten equation, in which disorder index I_v has a negative correlation with the characteristic curve index n.

Finally, the study of fluid drainage characteristics with various surface wettability demonstrates that the effect of microstructural disorder on residual volume is clearly weakened with the increase of hydrophobicity. In addition, when the surface wettability vary from hydrophilic to hydrophobic, morphological characteristics of highly-disordered topology have an obvious transformation from various saturated zones to only entrapped droplets.

In summary, this paper provides a fresh perspective into the significant applications of two-phase flows, in which displacement efficiency and morphological feature of wetting phase are crucial. For example, decreasing disorder degree can control the drainage processes, desirable for improving the displacement efficiency of water during drying of food and soil aeration processes, and accelerating the recovery of contaminants and CO_2 geosequestration. On the other hand, increasing disorder enlarges the interfacial area, which is advantageous for the subsurface remediation, fluid-gas mixing, and reaction enhancement in microfluidics.

5. Conclusions

Based on Voronoi tessellations of the pore space, the disorder index I_v has been introduced to describe the drainage characteristics in disordered porous media. With the help of this index, we studied the gravity-driven drainage with different pore configurations exhibiting a broad range of disorder degree. The results demonstrate that I_v is able to quantitatively characterize the influence of the disorder of porous media on the residual volume and morphological characteristics of residual saturated zones. Among other factors (capillarity, gravity, wettability, porosity and characteristic size), this study highlights the correlations between the disorder index to the following drainage behaviour: (1) residual saturation, (2) morphological features and (3) statistical distribution of residual wetting phase. The results presented in this paper contribute to fundamentally understand the physical principles behind multiphase flow in disordered porous media and to improve applications related to control and optimize the drainage processes.

Acknowledgement

This work was financially supported by Australian Research Council (Projects DP170102886) and The University of Sydney SOAR Fellowship.

Supplementary materials

Supplementary material associated with this article can be found, in the online version, at doi:10.1016/j.ijmultiphaseflow.2019.02.001.

References

Anguy, Y., et al., 2001. On the ability of a class of random models to portray the structural features of real, observed, porous media in relation to fluid flow. Cement Concr. Compos. 23 (2–3), 313–330.
Babadagli, T., et al., 2015. Effect of surface roughness and lithology on the water–gas and water–oil relative permeability ratios of oil-wet single fractures. Int. J. Multiph. Flow 75, 68–81.
Bandara, U.C., et al., 2011. Pore-scale study of capillary trapping mechanism during CO2 injection in geological formations. Int. J. Greenhouse Gas Control 5 (6), 1566–1577.
Birovljev, A., et al., 1991. Gravity invasion percolation in two dimensions: experiment and simulation. Phys. Rev. Lett. 67 (5), 584.
Blunt, M.J., Scher, H., 1995. Pore-level modeling of wetting. Phys. Rev. E 52 (6), 6387.
Boyce, C., et al., 2016. Intrusion of a liquid droplet into a powder under gravity. Langmuir 32 (34), 8631–8640.
Cieplak, M., Robbins, M.O., 1990. Influence of contact angle on quasistatic fluid invasion of porous media. Phys. Rev. B 41 (16), 11508.
Colombo, M., Fairweather, M., 2015. Multiphase turbulence in bubbly flows: RANS simulations. Int. J. Multiph. Flow 77, 222–243.
Dias, M.M., Payatakes, A.C., 1986. Network models for two-phase flow in porous media Part 1. Immiscible microdisplacement of non-wetting fluids.. J. Fluid Mech. 164, 305–336.
Fantinel, P., et al., 2017. Drying in a microfluidic chip: experiments and simulations. Sci. Rep. 7 (1), 15572.
Ferrari, A., et al., 2015. Challenges in modeling unstable two-phase flow experiments in porous micromodels. Water Resour. Res. 51 (3), 1381–1400.
Ferrari, A., Lunati, I., 2013. Direct numerical simulations of interface dynamics to link capillary pressure and total surface energy. Adv. Water Resour. 57, 19–31.
Fredlund, D.G., et al., 2012. Unsaturated Soil Mechanics in Engineering Practice. John Wiley & Sons.
Ghanbarian, B., et al., 2015. Gas and solute diffusion in partially saturated porous media: percolation theory and effective medium approximation compared with lattice Boltzmann simulations. J. Geophys. Res.: Solid Earth 120 (1), 182–190.
Greenshields, C.J., 2015. Openfoam User Guide, 3. OpenFOAM Foundation Ltd, version.
Herring, A.L., et al., 2016. Impact of wettability alteration on 3D nonwetting phase trapping and transport. Int. J. Greenhouse Gas Control 46, 175–186.
Holtzman, R., 2016. Effects of pore-scale disorder on fluid displacement in partially-wettable porous media. Sci. Rep. 6, 36221.
Horgue, P., et al., 2013. Experimental and numerical study of two-phase flows in arrays of cylinders. Chem. Eng. Sci. 102, 335–345.
Hu, R., et al., 2018. Wettability and flow rate impacts on immiscible displacement: a theoretical model. Geophys. Res. Lett. 45 (7), 3077–3086.
Islam, A., et al., 2014. Characterization of the crossover from capillary invasion to viscous fingering to fracturing during drainage in a vertical 2D porous medium. Int. J. Multiph. Flow 58, 279–291.
Laubie, H., et al., 2017b. Disorder-induced stiffness degradation of highly disordered porous materials. J. Mech. Phys. Solids 106, 207–228.

Laubie, H., et al., 2017a. Stress transmission and failure in disordered porous media. Phys. Rev. Lett. 119 (7), 075501.
Li, S., et al., 2018. Dynamics of viscous entrapped saturated zones in partially wetted porous media. Transp. Porous Media 125, 193–210.
Lin, J., et al., 2018. Experimental investigation of N2 injection to enhance gas drainage in CO 2-rich low permeable seam. Fuel 215, 665–674.
Liu, H., et al., 2015. Lattice Boltzmann simulation of immiscible fluid displacement in porous media: homogeneous versus heterogeneous pore network. Phys. Fluids 27 (5), 052103.
Løvoll, G., et al., 2005. Competition of gravity, capillary and viscous forces during drainage in a two-dimensional porous medium, a pore scale study. Energy 30 (6), 861–872.
March, R., et al., 2018. Assessment of CO2 storage potential in naturally fractured reservoirs with dual-porosity models. Water Resour. Res. 54 (3), 1650–1668.
Méheust, Y., et al., 2002. Interface scaling in a two-dimensional porous medium under combined viscous, gravity, and capillary effects. Phys. Rev. E 66 (5), 051603.
Moebius, F., Or, D., 2014. Pore scale dynamics underlying the motion of drainage fronts in porous media. Water Resour. Res. 50 (11), 8441–8457.
Moura, M., et al., 2015. Impact of sample geometry on the measurement of pressure-saturation curves: experiments and simulations. Water Resour. Res. 51 (11), 8900–8926.
Olivella, S., et al., 1994. Nonisothermal multiphase flow of brine and gas through saline media. Transp. Porous Media 15 (3), 271–293.
Owkes, M., Desjardins, O., 2014. A computational framework for conservative, three-dimensional, unsplit, geometric transport with application to the volume-of-fluid (VOF) method. J. Comput. Phys. 270, 587–612.
Pak, T., et al., 2015. Droplet fragmentation: 3D imaging of a previously unidentified pore-scale process during multiphase flow in porous media. In: Proceedings of the National Academy of Sciences, 112, pp. 1947–1952.
Parker, J., et al., 1987. A parametric model for constitutive properties governing multiphase flow in porous media. Water Resour. Res. 23 (4), 618–624.
Prat, M., 1995. Isothermal drying on non-hygroscopic capillary-porous materials as an invasion percolation process. Int. J. Multiph. Flow 21 (5), 875–892.
Rabbani, H.S., et al., 2017. New insights on the complex dynamics of two-phase flow in porous media under intermediate-wet conditions. Sci. Rep. 7 (1), 4584.
Rognmo, A., et al., 2017. Nanotechnology for improved CO2 utilization in CCS: laboratory study of CO2-foam flow and silica nanoparticle retention in porous media. Int. J. Greenhouse Gas Control 64, 113–118.
Succi, S., et al., 1989. Three-dimensional flows in complex geometries with the lattice Boltzmann method. EPL (Europhys. Lett.) 10 (5), 433.
Toussaint, R., et al., 2005. Influence of pore-scale disorder on viscous fingering during drainage. EPL (Europhys. Lett.) 71 (4), 583.
Woo, H.-J., et al., 2004. Modeling desorption of fluids from disordered mesoporous materials. Langmuir 20 (11), 4743–4747.
Yang, Y.-W., et al., 1988. Capillary flow phenomena and wettability in porous media: I. Static characteristics.. J. Colloid Interface Sci. 122 (1), 24–34.
Yekta, A., et al., 2018. Determination of hydrogen–water relative permeability and capillary pressure in sandstone: application to underground hydrogen injection in sedimentary formations. Transp. Porous Media 122 (2), 333–356.
Zhao, B., et al., 2016. Wettability control on multiphase flow in patterned microfluidics. In: Proceedings of the National Academy of Sciences, 113, pp. 10251–10256.
Zhou, A., et al., 2016. Capillary water retention curve and shear strength of unsaturated soils. Can. Geotech. J. 53 (6), 974.